Equatorial waves, diurnal tides and small-scale thermal variability in the tropical lower stratosphere from COSMIC-2 radio occultation

William J. Randel[1,2] and Fei Wu[1]

[1]National Center for Atmospheric Research, Boulder, CO, USA

[2]COSMIC Program, University Corporation for Atmospheric Research, Boulder, CO, USA

September 2020

Key points:

- Tropical temperature variability is quantified using dense COSMIC-2 radio occultation measurements

- COSMIC-2 data reveal a rich spectrum of equatorial planetary waves and diurnal tides in the tropical lower stratosphere

- Small-scale temperature variances reveal coherent geophysical structures tied to convection and stratospheric Kelvin waves

Abstract

A new constellation of radio occultation satellites called COSMIC-2 (Constellation Observing System for Meteorology, Ionosphere and Climate-2) is providing unprecedented dense measurements of the tropical atmosphere, with on average more than 4,000 high quality observations per day over 40^o N-S. We use these data to evaluate large- and small-scale thermal variability in the tropical lower stratosphere during October 2019 – April 2020. Space-time spectral analysis of gridded COSMIC-2 data reveals a rich spectrum of traveling planetary-scale waves, including Kelvin waves, mixed Rossby-gravity waves and inertia gravity waves, in addition to propagating diurnal tides. These coherent modes show enhanced amplitudes from the tropical tropopause through the lower stratosphere (~17-25 km). Characteristics of small-scale temperature variances, calculated as deviations from the gridded fields, reveal systematic spatial patterns including time average maxima over Africa and South America overlying persistent deep convection. Small-scale variances also exhibit transient maxima in the equatorial lower stratosphere tied to large-scale Kelvin waves. The new COSMIC-2 observations provide novel details on the rich spectrum of large- and small-scale waves near and above the tropical tropopause.

Plain Language Summary

A new constellation of radio occultation satellites called COSMIC-2 (Constellation Observing System for Meteorology, Ionosphere and Climate-2) is providing unprecedented dense measurements of the tropical atmosphere, with on average more than 4,000 high quality observations per day over 40^o N-S. We use these data to provide novel understanding of temperature variability near the tropical tropopause and lower stratosphere (~10-30 km). COSMIC-2 data reveal a rich spectrum of large- and small-scale waves, including eastward- and westward-propagating planetary-scale equatorial waves and diurnal tides. The measurements also identify localized regions of enhanced temperature variability tied to small-scale gravity waves. These new measurements are valuable for constraining global models and understanding high-level clouds in the tropics.

Introduction

Large-scale equatorial waves contribute a dominant fraction of variance for meteorological fields in the tropical upper troposphere and lower stratosphere (UTLS). These waves are important for their organized contributions to UTLS circulation, constituent transport and cloud formation processes, e.g. Fujiwara et al, 2001; 2009; Mote and Dunkerton, 2004; Jensen and Pfister, 2004; Kim et al, 2016. Additionally, UTLS equatorial waves propagate vertically and provide important forcing for the stratospheric quasi-biennial oscillation (QBO) and semi-annual oscillation (SAO), and hence it is important to quantify wave behavior in observations and use measurements to evaluate and constrain models (e.g. Kawatani et al, 2009; Holt et al, 2016; 2020).

Satellites provide key observations for characterizing equatorial waves. An important aspect of equatorial waves is their relatively narrow vertical scales (typical vertical wavelengths of ~4-8 km), so that high vertical resolution is important for satellite measurements. Temperature retrievals from Global Navigation Satellite System (GNSS) radio occultation (RO) have UTLS vertical resolution of ~ 1 km or better (Zeng et al, 2019), and global measurements since ~2002 have provided characterization of equatorial wave structure and long-term variability (e.g. Tsai et al, 2004; Randel and Wu, 2005; Alexander et al, 2008; Kim and Son, 2012; Scherllin-Pirscher et al, 2017). Complementary studies with other high resolution satellite data were provided by Ern et al (2008) and Alexander and Ortland (2010), and numerous studies have analyzed UTLS equatorial waves in meteorological reanalyses (e.g. Kim et al, 2019, and references therein).

The focus of this work is an analysis of thermal variability in the tropical lower stratosphere using the dense, high quality RO measurements from the COSMIC-2 constellation, launched in June 2019. COSMIC-2 (hereafter C2) is a set of 6 satellites in low inclination Earth orbit, which will provide ~5,000 occultations per day over low latitudes (40^{o} N-S) when fully operational. C2 satellites have improved receivers that provide enhanced signal-to-noise ratio compared to previous RO missions (Schreiner et al, 2020), and we use the high quality data to provide a novel look at UTLS thermal variability during the first several months of observations (October 2019 – April 2020). In addition to analyses of large-scale gridded fields, the concentrated sampling of C2 provides opportunity to evaluate smaller-scale variability (i.e.

deviations from the analyzed large-scale structure), and we highlight interesting coherent behavior of the small scale temperature variances in these new data.

2. Data and Analyses

The six-satellite C2 constellation has been providing on average more than 4,000 RO profiles per day since September 2019 (Schreiner et al, 2020). The C2 satellites are in low inclination orbits, providing observations over low latitudes out to ~40^o N-S, with ~ 70% of the measurements over the deep tropics 20^o N-S. We analyze C2 temperature profiles (so-called dry temperature retrievals, atmPrf) over altitudes 10-30 km sampled at 200 m vertical resolution for the period October 2019 – April 2020, using data obtained from the COSMIC Data Analysis and Archive Center (CDACC) website https://cdaac-www.cosmic.ucar.edu/. Our focus is on the thermal wave variability in the UTLS region ~15-25 km. Stratospheric winds have a strong influence on UTLS equatorial waves (e.g. Kawatani et al, 2009; Kim et al, 2019), in particular wind variations tied to the QBO. During the period studied here the lower stratospheric zonal winds were evolving from weak westerly to weak easterly winds over altitudes ~17-25 km, with stronger easterly winds above 25 km (see https://acd-ext.gsfc.nasa.gov/Data_services/met/qbo/qbo.html).

In order to study large-scale waves including extension to diurnal variability, we derive a 6-hourly gridded version of the C2 temperature data on a 4^o latitude by 10^o longitude (ϕ,λ) grid, using a Gaussian-weighted average (in longitude and time) of the individual GPS measurements, following Randel and Wu (2005). Gridded temperatures are calculated as $T_{grid}(\lambda,t) = \Sigma\, w_i T_i / \Sigma\, w_i$, with T_i the individual C2 measurements (within +/- 2^o of each grid latitude) and $w_i = \exp(-[(\Delta\lambda/D)^2+(\Delta t/T)^2])$ is a Gaussian weighting function in longitude and time. Here $\Delta\lambda$ is the difference between the grid center and each C2 measurement, Δt the corresponding time difference, D=2^o and T=1 hour. The parameters D and T are empirically chosen to provide reasonable gridding and spectral analysis results, and this mapping provides a straightforward method to grid the irregular C2 data and smooth the dense grid over short data voids. Figure 1 shows an example of C2 sampling near the equator for one day (January 14, 2020), along with the resulting gridded temperature field. Results in Fig. 1 highlight strong zonal temperature structure with patterns centered over the equator (e.g. the cold region near ~180^o), which is associated with an equatorial Kelvin wave that is known to dominate variability near the tropical tropopause (e.g. Kim and Son, 2012; Scherllin-Pirscher et al, 2017).

In order to identify coherent large-scale wave behavior we perform zonal wavenumber-frequency cross-spectrum analysis of the gridded temperature data for the 120-day period November 1, 2019 to February 28, 2020 (with 4x daily time samples), using the standard formulation of Hayashi (1982). Following previous studies (e.g. Wheeler and Kiladis, 1999; Alexander et al, 2008; Kawatani et al, 2009) we analyze the gridded temperature wave structures that are symmetric (S) and antisymmetric (AS) about the equator as $T_S = (T(\phi) + T(-\phi))/2$ and $T_{AS} = (T(\phi) - T(-\phi))/2$, with averages over latitudes 0-16°. We note that our results show actual temperature wave power, not ratios of power compared to a smoothed background spectrum as in Wheeler and Kiladis (1999).

We also analyze the ‘residual’ temperature, which is defined as the difference between the C2 profile measurements and the gridded temperature fields, $T_{res} = T_i - T_{grid}$. For these calculations we take the daily average gridded values, and calculate daily average residual variances. These differences represent small-scale variability, such as that due to gravity waves, that is not captured in the gridded temperature fields. Examples of this variability are evident in Fig. 1a as the differences between the individual data points and the smooth gridded field. Similar analyses (differences from horizontally gridded fields) have been used to identify the statistical structure of small-scale gravity waves in RO data by e.g. Wang and Alexander, 2010, Schmidt et al, 2016 and Xu et al, 2018.

3. Results

3.1 Resolved equatorial waves and tides

Time series of zonal temperature variance at 18 km over 8° N-S from C2 data are shown in Fig. 2, including total variance calculated from the full individual C2 measurements ($\sigma^2_{total} = \Sigma (T_i - T_{bar})^2$), the gridded field ($\sigma^2_{grid} = \Sigma (T_{grid} - T_{bar})^2$) and the residual ($\sigma^2_{resid} = \sigma^2_{total} - \sigma^2_{grid}$), with T_{bar} the zonal average. Zonal temperature variance exhibits several maxima throughout the period, and the majority of the variance is captured by the gridded component, i.e. most of the temperature variability is associated with large-scale waves resolved by the 10° longitude grid.

The zonal mean residual variance in Fig. 2b is relatively constant in time, and is as energetic as the gridded field when the large-scale waves are quiescent. Further details of the residual are discussed below.

As is well-known, the large-scale temperature fields in the tropical lower stratosphere are dominated by Kelvin waves (e.g. Alexander et al, 2008; Kim and Son, 2012; Scherllin-Pirscher et al, 2017). This behavior is characterized by eastward traveling planetary-scale waves with period near 20 days, as shown for the gridded C2 data at 18 km in Fig. 3a. Quasi-stationary waves are also observed near longitudes 180 - 240^o in Fig. 3a, which are climatological features (Scherllin-Pirscher et al, 2017). Snapshots of Kelvin wave vertical structure are analyzed further below, showing a characteristic eastward phase tilt with height and a typical vertical wavelength near ~6 km. Kelvin waves account for a majority of the gridded (and total) temperature variance throughout the season in Fig. 2b. Figure 3b shows longitude-time evolution of the residual temperature variance at 18 km, which will be discussed further in Section 3b.

Zonal wavenumber-frequency temperature power spectra for symmetric and antisymmetric equatorial temperatures at 20 km are shown in Fig. 4, and similar spectra are found for altitudes from the tropopause throughout the lower stratosphere (~17-25 km). Spectra are shown for frequencies 0 – 1.3 cycles per day (cpd), as higher frequencies (out to 2.0 cpd) are poorly resolved in the 6-hour grids. Symmetric power (Fig. 4a) is dominated by eastward traveling Kelvin waves, with spectral peaks out to zonal wavenumber 4 and beyond, along with low frequency westward moving planetary-scale waves consistent with equatorial Rossby waves. Figure 4 includes theoretical equatorial wave dispersion curves for several different equatorial wave modes and vertical wavelengths (4, 6 and 8 km), with labeling following standard nomenclature, e.g. Wheeler and Kiladis, 1999 (here 'n' is the meridional mode index). These theoretical dispersion curves show reasonable agreement with the observed power spectra. The symmetric spectra (Fig. 4a) also shows a weak maximum for westward moving waves with period 2-3 days, consistent with higher order n=1 inertia gravity (IG) waves.

Antisymmetric power spectra (Fig. 4b) show peaks for westward moving waves ~1-5 with periods ~4-6 days, linked to mixed Rossby-gravity (MRG) waves, along with higher frequency (~2.5 – 4 day) eastward traveling planetary scales (n=0 IG waves). These antisymmetric temperature waves are consistent with previous observations in the lower stratosphere, e.g. Alexander et al, 2008; Alexander and Ortland, 2010, Kiladis et al, 2016, and the maxima are especially distinct in the spectra derived from high density C2 measurements. The observed spectra in Fig. 4b agree best with the theoretical dispersion curves for vertical wavelengths ~ 4-6 km.

Both the symmetric and antisymmetric spectra in Fig. 4 show a diurnal peak (frequency near 1.0 cpd) for westward moving zonal wave 1, which is the well-known migrating (or sun-synchronous) diurnal tide (so-called DW1). The migrating diurnal tide has been isolated in multi-year records of radio occultation measurements by Zeng et al (2008), Pirscher et al (2010) and Xie et al (2010), and shows up clearly in this relatively short record from C2. Amplitude and phase structure of the diurnal tide is discussed below. In the lower stratosphere the DW1 amplitude is maximum over ~20^o S to 0^o (during this boreal winter season), with a resulting projection onto symmetric and antisymmetric components in Fig. 4.

Latitudinal structure of the various equatorial wave modes is illustrated for the 20 km level in Fig. 5, combining power from zonal wavenumbers 1-6. Similar patterns are found at all levels throughout the lower stratosphere. The eastward Kelvin wave dominates power near the equator, with a symmetric maximum over ~10^o N-S. Westward MRG waves show distinctive ~4-6 day period maxima near ~8^o N and S which are out of phase (antisymmetric). Weaker but identifiable antisymmetric maxima are also seen for n=0 eastward IG waves near ~3 day period, along with a symmetric n=1 westward peak over the equator near 2-3 days period. Vertical structure of the symmetric and antisymmetric power for combined wavenumbers 1-6 (Figs. 6a-b) reveal each of the spectral peaks discussed above, and show that the waves extend from approximately the tropopause (17 km) to above 25 km, and to higher altitudes for the Kelvin waves and DW1 tide. The MRG waves in Fig. 6b show a systematic shift to higher frequencies at higher altitude, and this behavior is consistent with absorption of lower frequencies (slower phase speeds) as the waves propagate vertically from the tropopause level through weak zonal mean westerly winds.

In addition to the westward DW1 diurnal tide, Fig. 5 furthermore reveals spectral peaks for *eastward* propagating diurnal oscillations at latitudes poleward of ~15^o N and S. These are associated with non-migrating tides with maxima for zonal wavenumbers 1-4 in the C2 data, although we note larger uncertainty for spectrum analysis of diurnal oscillations from C2 sampling at extratropical latitudes. We term this the DE1/4 mode in analogy to the non-migrating eastward zonal wave 3 mode (DE3) often observed in the middle atmosphere (e.g. Forbes et al, 2006). The eastward non-migrating tides are likely forced by the diurnal cycle of spatially-fixed convective heating in the tropical troposphere (Hagan and Forbes, 2002); the DE3 tidal oscillations propagate vertically and reach large amplitudes in the mesosphere and lower thermosphere, and feature prominently in coupling the lower and upper atmosphere (e.g. Forbes et al, 2006). Spatial structure of the rms amplitudes of DW1 and DE1/4 derived from C2 data are shown in Fig. 7, with rms amplitudes defined as $A_{rms} = (2*T_{var})^{1/2}$, with temperature variance T_{var} calculated as spectral power integrated over frequencies 0.9 – 1.1 cpd, for westward zonal wave 1 (DW1) and eastward zonal waves 1-4 (DE1/4). Amplitude of DW1 (Fig. 7a) is similar to that shown in Zeng et al (2008), with maximum centered in low latitudes increasing in amplitude from ~0.1 K near the tropopause to ~ 0.5 K at 30 km. The corresponding phase (not shown) decreases regularly (occurs earlier) at higher altitudes, e.g. Zeng et al, 2008. Spatial structure of the eastward DE1/4 tide (Fig. 7b) is very different from DW1, with temperature amplitudes of ~0.3-0.4 K polewards of ~15^o N and S, and maxima over ~15-20 km and also below ~12 km. The extratropical maxima for individual waves 1-3 are statistically coherent and out-of-phase between hemispheres (not shown).

3.2 Residual temperature variance

The residual temperature variance represents small scales that are below the 10^o longitude and 6-hour time resolutions of the gridded fields, and we examine space-time structure by calculating the variance of the C2 residuals within each 4^o x 10^o grid box, calculated for daily samples. The time average (December 2019 – February 2020) residual variance for the 18-20 km layer is shown in Fig. 8, revealing coherent spatial maxima that are suggestive of actual geophysical variability. In the deep tropics, residual variance shows isolated maxima over Africa and S. America (~16^o S to 0^o) that are likely associated with small-scale gravity waves forced by the underlying persistent continental convection. Figure 8 also shows a broad longitudinal maximum in variance near the equator over the Indian and Pacific oceans that could be linked with underlying low latitude convection and/or shear structures in the large-scale flow, as explored further below. The residual temperature variance in Fig. 8 furthermore shows maxima over continental regions in the extratropics, including a large maximum over and downstream of

Asia and over North America. These could possibly be related to gravity waves in the lower stratosphere generated by flow over topography, e.g. Wang and Geller, 2003. There are also maxima in the Southern Hemisphere over Australia and over the Andes (~300^{o}), and the latter is a well-known hot spot for stratospheric gravity wave activity, e.g. Eckerman and Preusse, 1999. The presence of coherent spatial structures in the time average statistics in Fig. 8 argues that the temperature residuals calculated in a simple manner from C2 data represent actual geophysical variability.

Space-time variations of residual variance in the tropical UTLS furthermore shows coherence with the large-scale Kelvin waves. Figure 3b shows the residual variance over the equator at 18 km as a function of longitude and time, highlighting episodic eastward traveling maxima that are closely related to the ‘background’ large-scale Kelvin waves in Fig. 3a. Dashed lines in Figs. 3a-b show that localized residual variance maxima occur in the longitudinal shear zones of the background Kelvin wave temperatures; maxima also occur with respect to vertical shear zones for Kelvin waves. The spatial relationships between the residual variance and the gridded temperature anomalies, and their evolution for several example days in January and March 2020 are highlighted in Fig. 9. These examples show residual variance maxima sandwiched between large positive and negative temperature patterns associated with Kelvin waves, with the enhanced residuals following the eastward slope with altitude and phase progression with time. Another way to state this is that enhanced small-scale temperature fluctuations are observed close to large zonal (and vertical) Kelvin wave temperature gradients, and an example of this enhanced variability is seen in the individual C2 measurements over longitudes ~140^{o}-170^{o} in Fig. 1a (for the same day as in Fig. 9b). A speculative physical interpretation could be that enhanced small-scale waves (gravity waves) are tied to the strong Kelvin wave shear zones, either through in situ forcing from shear instabilities (e.g. Fujiwara et al, 2003; Flannaghan and Fueglistaler, 2011) or wave propagation effects through the varying vertical shear flow. Whatever the explanation, the dense C2 observations clearly show close coupling of the transient small-scale temperature variance with the large scale Kelvin waves, in addition to coherent spatial structure of the time averages seen in Fig. 8.

4. Summary and discussion

The concentrated space-time sampling of high vertical resolution temperature retrievals from C2 allows a novel analysis of large- and small-scale temperature variability in the tropical UTLS. The large-scale gridded results from C2 show the well-known dominance of eastward moving planetary-scale Kelvin waves with periods near 20 days, in addition to strong westward traveling MRG waves (zonal waves ~1-5, periods ~4-6 days). The MRG waves have smaller (antisymmetric) tropical temperature amplitudes than the symmetric Kelvin waves, but are important for equatorial meridional wind and westward momentum fluxes into the lower stratosphere (e.g. Kim et al, 2019). The C2 data also show evidence for small amplitude inertia-gravity waves, both eastward and westward modes with ~2-3 days period and distinctive meridional structures, which are interesting but less important for upward momentum fluxes (Kawatani et al, 2010). Our analyses reveal the westward migrating zonal wave 1 diurnal tide (DW1) with maximum amplitude in the tropical stratosphere, as found in previous studies with RO data (Zeng et al, 2008). A new finding here is enhanced power for eastward non-migrating diurnal tides at extratropical latitudes in the troposphere and lower stratosphere of both hemispheres (Figs. 5 and 7b), with the majority of power at zonal waves 1-4 (DE1/4). The C2 sampling does not allow characterization of this behavior at higher latitudes, but that might be achieved in the future by combining RO measurements from additional satellites.

We have also explored the systematic behavior of small-scale ('residual') temperature variances in C2 measurements, based on subtracting the large-scale gridded temperature field. These residuals are probably associated with small-scale gravity waves. As noted above, our separation of small scales based on differences with horizontal gridded fields is similar to previous studies (e.g. Wang and Alexander, 2010), and is a complement to separation based on filtering vertical profiles. Despite a relatively short time sample, the C2 residual variances exhibit coherent space-time structure that is suggestive of actual geophysical behavior. Time averages in the lower stratosphere (Fig. 8) show maxima over Africa and South America that are consistent with forcing from persistent tropical convection, in addition to maxima over midlatitude continents that may be linked to orography and/or convective sources. Further studies of the detailed time variability in these regions may be interesting. Lower stratosphere residuals also maximize over the equatorial Indian and Pacific oceans, and here the small-scale variance is organized in regions linked to traveling shear zones of the background large-scale

Kelvin waves (Figs. 3 and 9). The cause of this behavior is not well understood at present, but the coherent space-time patterns are suggestive of actual geophysical variability.

Our analyses have shown a snapshot of equatorial wave variability for the first several months of C2 observations, and it will be interesting to extend analyses to longer time periods to quantify links to tropospheric forcing and sensitivity to background stratospheric winds. These results may also be useful for detailed comparisons to meteorological reanalyses (especially before the assimilation of C2 data) and with high resolution global model simulations (e.g. Holt et al, 2020). As a note, the time period analyzed here also overlaps the recent Strateole2 long-duration balloon measurements made in the tropical lower stratosphere during November 2019 – February 2020 (https://webstr2.lmd.polytechnique.fr/#/), and the C2 observations may be useful to provide a global context to the high resolution balloon measurements.

Acknowledgements

The National Center for Atmospheric Research is sponsored by the U.S. National Science Foundation. This work has been partially supported by the COSMIC NSF/NASA Cooperative Agreement. COSMIC-2 data were obtained from the COSMIC Data Analysis and Archive Center (CDACC) website https://cdaac-www.cosmic.ucar.edu/. We thank Rolando Garcia, Rick Anthes and Ben Johnston for discussions and comments on the manuscript.

References

Alexander, M. J., & Ortland, D. A. (2010). Equatorial waves in High Resolution Dynamics Limb Sounder (HIRDLS) data. J. Geophys. Res. Atmos., 115 (D24111), doi: 10.1029/2010JD014782

Alexander, S. P., Tsuda, T., Kawatani, Y., & Takahashi, M. (2008). Global distribution of atmospheric waves in the equatorial upper troposphere and lower stratosphere: COSMIC observations of wave mean flow interactions. J. Geophys. Res., 113 (D24), D24115. doi: 10.1029/2008JD010039

Eckerman, S.D. and P. Preusse (1999). Global measurements of stratospheric mountain waves from space. Science, 286, 1534-1537, doi:10.1126/science.286.5444.1534

Ern, M., Preusse, P., Krebsbach, M., Mlynczak, M. G., and Russell III, J. M. (2008). Equatorial wave analysis from SABER and ECMWF temperatures, Atmos. Chem. Phys., 8, 845–869, https://doi.org/10.5194/acp-8-845-2008.

Flannaghan, T. J., and Fueglistaler, S. (2011). Kelvin waves and shear-flow turbulent mixing in the TTL in (re-)analysis data. *Geophysical Research Letters*, **38**.

Forbes, J. M., J. Russell, S. Miyahara, X. Zhang, S. Palo, M. Mlynczak, C. J. Mertens, and M. E. Hagan (2006). Troposphere-thermosphere tidal coupling as measured by the SABER instrument on TIMED during July–September 2002, J. Geophys. Res., 111, A10S06, doi:10.1029/2005JA011492.

Fujiwara, M., Hasebe, F., Shiotani, M., Nishi, N., Vömel, H., and Oltmans, S. J. (2001). Water vapor control at the tropopause by equatorial Kelvin waves observed over the Galápagos, Geophys. Res. Lett., 28, 3143–3146, https://doi.org/10.1029/2001GL013310.

Fujiwara, M., M. K. Yamamoto, H. Hashiguchi, T. Horinouchi, and S. Fukao (2003). Turbulence at the tropopause due to breaking Kelvin waves observed by the Equatorial Atmosphere Radar, Geophys. Res. Lett. , 30 (4), 1171, doi:10.1029/2002GL016278.

Fujiwara, M., et al. (2009). Cirrus observations in the tropical tropopause layer over the western Pacific, J. Geophys. Res., 114, D09304, doi:10.1029/2008JD011040

Hagan, M. E., and Forbes, J. M. (2002). Migrating and nonmigrating diurnal tides in the middle and upper atmosphere excited by tropospheric latent heat release. J. Geophys. Res.,107(D24), 4754, doi:10.1029/2001JD001236.

Hayashi, Y. (1982). Space-time spectral analysis and its application to atmospheric waves. J. Meteor. Soc. Japan, 60, 156-171.

Holt, L. A., Alexander, M. J., Coy, L., Molod, A., Putman, W., & Pawson, S. (2016). Tropical waves and the quasi-biennial oscillation in a 7-km global climate simulation. J. Atmos. Sci., 73 . doi: 10.1175/JAS-D-15-0350.1

Holt, L. A., Lott, F., Garcia, R. R., Kiladis, G. N., Cheng, Y.-M., Anstey, J. A.,. . . Yukimoto, S. (2020). An evaluation of tropical waves and wave forcing of the QBO in the QBOi models. Q. J. R. Meteorol. Soc., (In Press). doi:10.1002/qj.3827

Jensen, E., and L. Pfister (2004). Transport and freeze-drying in the tropical tropopause layer, J. Geophys. Res., 109, D02207, doi:10.1029/2003JD004022

Kawatani, Y., M. Takahashi, K. Sato, S. P. Alexander, and T. Tsuda (2009). Global distribution of atmospheric waves in the equatorial upper troposphere and lower stratosphere: AGCM simulation of sources and propagation, J. Geophys. Res., 114, D01102, doi:10.1029/2008JD010374.

Kawatani, Y., K. Sato, T. J. Dunkerton, S. Watanabe, S. Miyahara, and M. Takahashi (2010). The roles of equatorial trapped waves and internal inertia–gravity waves in driving the quasi-biennial oscillation. Part I: Zonal mean wave forcing. J. Atmos. Sci., 67, 963–980.

Kiladis, G.N., Dias, J. and Gehne, J. (2016). The Relationship between Equatorial Mixed Rossby–Gravity and Eastward Inertio-Gravity Waves. Part I. J. Atmos. Sci., 73, 2123-2145.

Kim, J., and S.-W. Son (2012). Tropical cold-point tropopause: Climatology, seasonal cycle, and intraseasonal variability derived from COSMIC GPS radio occultation measurements. J. Climate, 25 (15), 5343–5360, doi:10.1175/JCLI-D-11-00554.1.

Kim, J.-E., M. J. Alexander, T. P. Bui, J. M. Dean-Day, R. P. Lawson, S. Woods, D. Hlavka, L. Pfister, and E. J. Jensen (2016). Ubiquitous influence of waves on tropical high cirrus clouds, Geophys. Res. Lett., 43, 5895–5901, doi:10.1002/2016GL069293.

Kim, Y.-H., Kiladis, G. N., Albers, J. R., Dias, J., Fujiwara, M., Anstey, J. A., Song, I.-S., Wright, C. J., Kawatani, Y., Lott, F., and Yoo, C. (2019). Comparison of equatorial wave activity in the tropical tropopause layer and stratosphere represented in reanalyses, Atmos. Chem. Phys., 19, 10027–10050, https://doi.org/10.5194/acp-19-10027-2019

Mote, P. W., and T. J. Dunkerton (2004). Kelvin wave signatures in stratospheric trace constituents, J. Geophys. Res., 109, D03101, doi:10.1029/2002JD003370

Pirscher, B., U. Foelsche, M. Borsche, G. Kirchengast, and Y.-H. Kuo (2010). Analysis of migrating diurnal tides detected in FORMOSAT-3/COSMIC temperature data. J. Geophys. Res., 115, D14108, doi:10.1029/2009JD013008

Randel, W. J., and F. Wu (2005). Kelvin wave variability near the equatorial tropopause observed in GPS radio occultation measurements. J. Geophys. Res., 110, D03102, doi:10.1029/2004JD005006.

Scherllin-Pirscher, B., W. J. Randel, and J. Kim (2017). Tropical temperature variability and Kelvin-wave activity in the UTLS from GPS RO measurements. Atmos. Chem. Phys., 17, 793–806, doi:10.5194/acp-17-793-2017

Schmidt, T., P. Alexander, and A. de la Torre (2016). Stratospheric gravity wave momentum flux from radio occultation. J. Geophys. Res., 121, 4443–4467, doi:10.1002/2015JD024135.

Schreiner, W. S., Weiss, J. P., Anthes, R. A., Braun, J., Chu, V., Fong, J., et al. (2020). COSMIC-2 radio occultation constellation: First results. *Geophysical Research Letters*, *47*, e2019GL086841. https://doi.org/10.1029/2019GL086841

Tsai, H.-F., T. Tsuda, G. A. Hajj, J. Wickert, and Y. Aoyama (2004). Equatorial Kelvin waves observed with GPS occultation measurements (CHAMP and SAC-C). J. Meteor. Soc. Jpn., 82 (1B), 397–406.

Wang, L., and M. J. Alexander (2010). Global estimates of gravity wave parameters from GPS radio occultation temperature data. J. Geophys. Res., 115, D21122, doi:10.1029/2010JD013860.

Wang, L., and M. A. Geller (2003). Morphology of gravity-wave energy as observed from 4 years (1998–2001) of high vertical resolution U.S. radiosonde data, J. Geophys. Res., 108(D16), 4489, doi:10.1029/2002JD002786.

Wheeler, M., and G. N. Kiladis (1999). Convectively coupled equatorial waves: Analysis of clouds and temperature in the wavenumber–frequency domain. J. Atmos. Sci., 56, 374–399.

Xie, F., D. L. Wu, C. O. Ao, and A. J. Mannucci (2010). Atmospheric diurnal variations observed with GPS radio occultation soundings. Atmos. Chem. Phys., 10, 6889–6899, doi:10.5194/acp-10-6889-2010.

Xu, X., D. Yu, and J. Luo (2018). The spatial and temporal variability of global stratospheric gravity waves and their activity during sudden stratospheric warming revealed by COSMIC measurements. Adv. Atmos. Sci., 35 (12), 1533–1546, doi:10.1007/s00376-018-5053-1.

Zeng, Z., W. Randel, S. Sokolovskiy, C. Deser, Y.-H. Kuo, M. Hagan, J. Du, and W. Ward (2008). Detection of migrating diurnal tide in the tropical upper troposphere and lower stratosphere using the ChallengingMinisatellite Payload radio occultation data. J. Geophys. Res., 113, D03102, doi:10.1029/2007JD008725

Zeng, Z., S. Sokolovskiy, W.S. Schreiner, and D. Hunt (2019). Representation of vertical structures by radio occultation observations in the upper troposphere and lower stratosphere. Comparison to high-resolution radiosonde profiles. J. Atmos. and Oceanic Tech., https://doi.org/10.1175/JTECH-D-18-0105.1

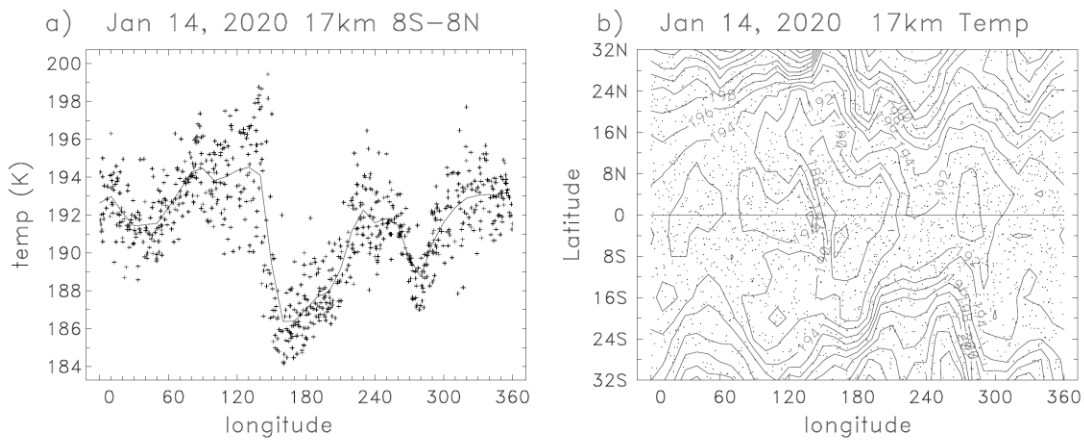

Figure 1. (a) Individual C2 temperature measurements at 17 km over 8^o N-S for January 14, 2020. The thin line shows the associated gridded temperature field. (b) Gridded spatial structure of temperatures at 17 km on this day, with the dots indicating the C2 measurement locations.

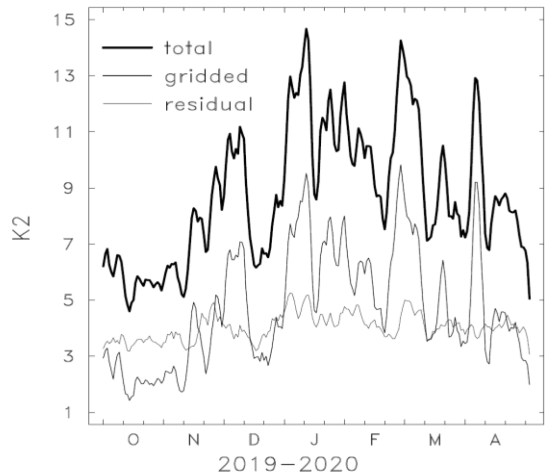

Figure 2. Time series of zonal temperature variance (K^2) at 18 km over 8^o N-S, calculated from the full C2 measurements (total), from the gridded fields and the residual (difference between the total and gridded results).

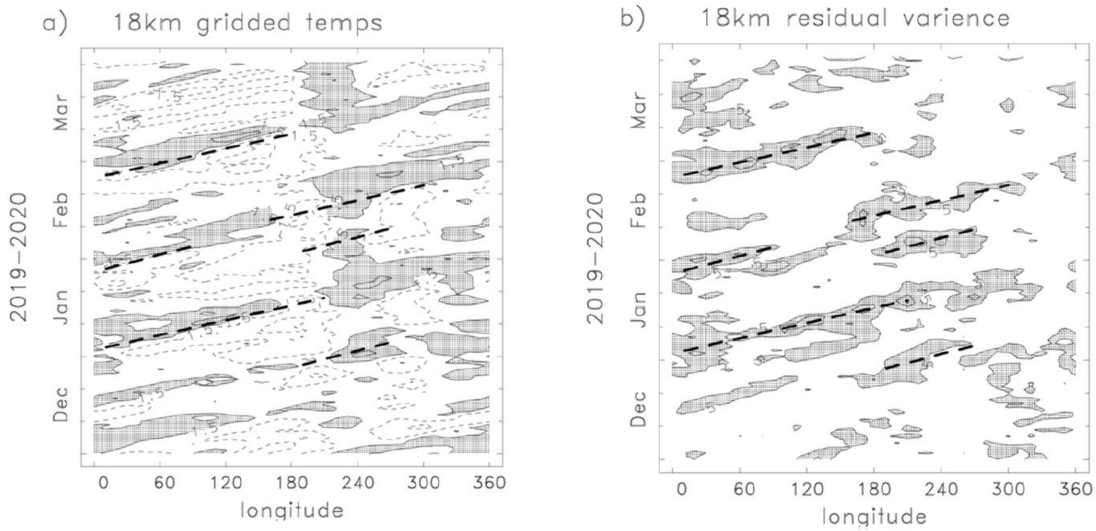

Figure 3. (a) Longitude-time diagram of gridded temperature anomalies over the equator (8^o N-S) at 18 km (contours of +/- 1.5, 4.5 K) highlighting eastward traveling Kelvin waves. (b) Residual temperature variance over 8^o N-S at 18 km, with contour interval of 5 K^2. The thick dashed lines in both panels follow some of the residual variance maxima.

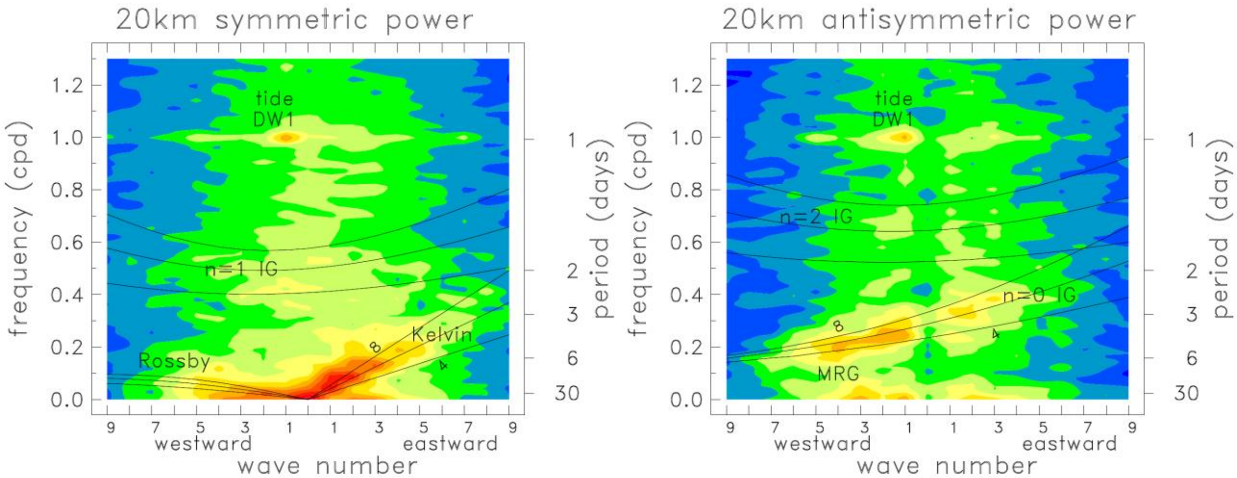

Figure 4. Zonal wavenumber-frequency power spectra at 20 km for (a) symmetric and (b) antisymmetric equatorial waves over 0-16^{o} N-S, derived from gridded C2 data. The color scale is shown in Fig. 5. The black lines denote equatorial wave dispersion curves for symmetric and antisymmetric waves, following e.g. Wheeler and Kiladis, 1999, and displayed for a set of vertical wavelengths 4, 6 and 8 km. Labels indicate maxima associated with various wave modes, including equatorial Rossby, Kelvin, mixed Rossby-gravity (MRG), inertia-gravity (IG) waves and migrating diurnal tide (DW1).

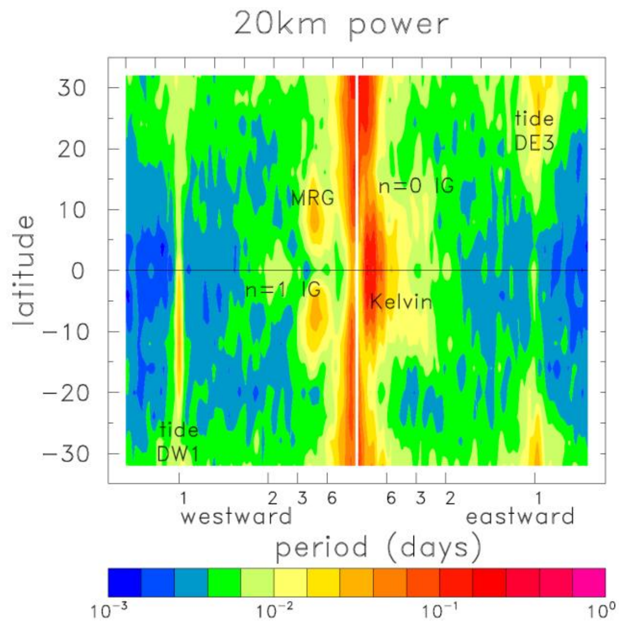

Figure 5. (a) Eastward-westward power spectra at 20 km as a function of latitude for combined zonal waves 1-6. Labels indicate various equatorial modes, as in Fig. 4.

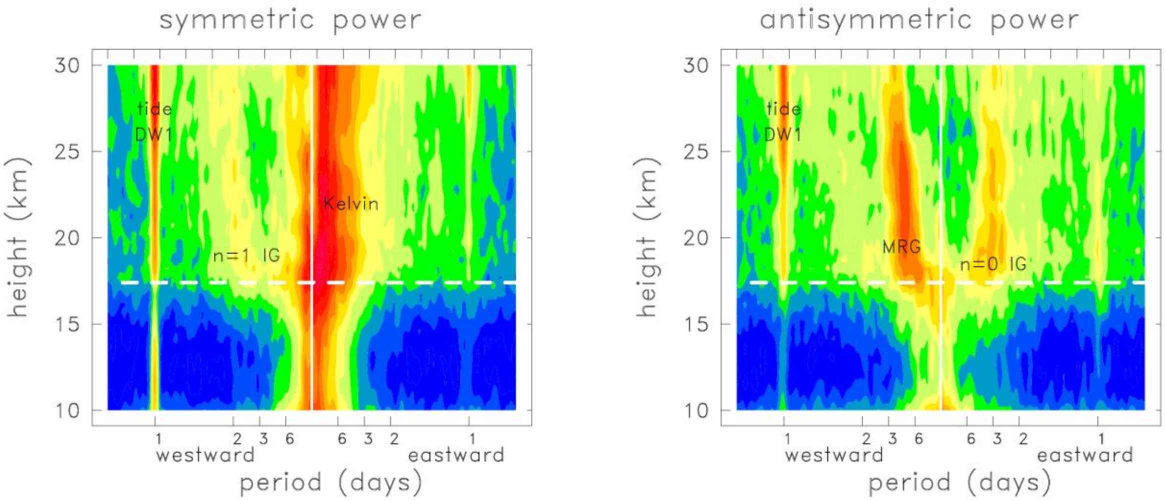

Figure 6. Height vs. frequency power spectra for combined zonal waves 1-6, for symmetric (a) and antisymmetric (b) components. Color bar is the same as in Fig. 5. Labels indicate various wave modes, as in Figs. 4-5. The white dashed lines indicate the tropopause altitude.

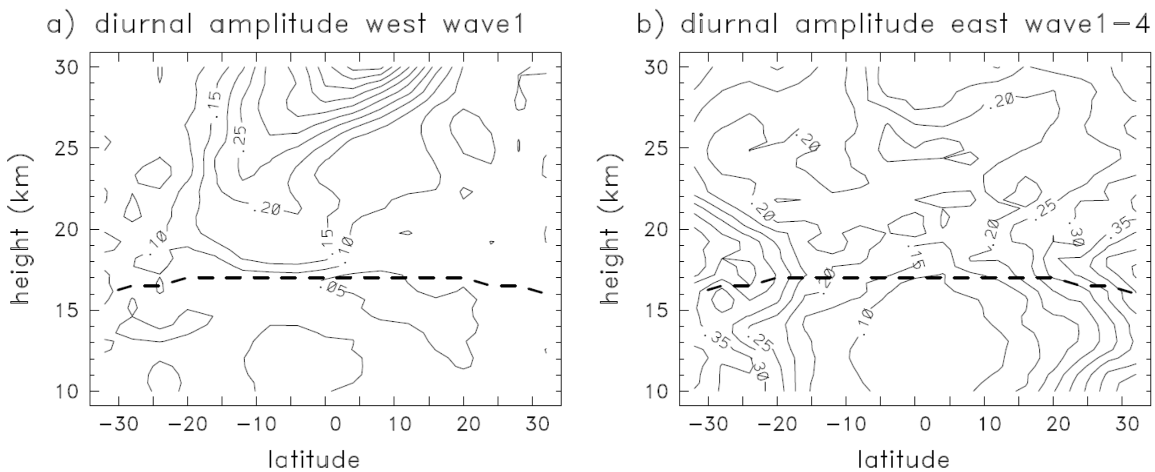

Figure 7. Meridional cross sections of rms amplitude for (a) migrating diurnal tide DW1, and (b) non-migrating diurnal tide DE1/4 (discussed in text). Contour interval is 0.05 K. The dark dashed line is the thermal tropopause.

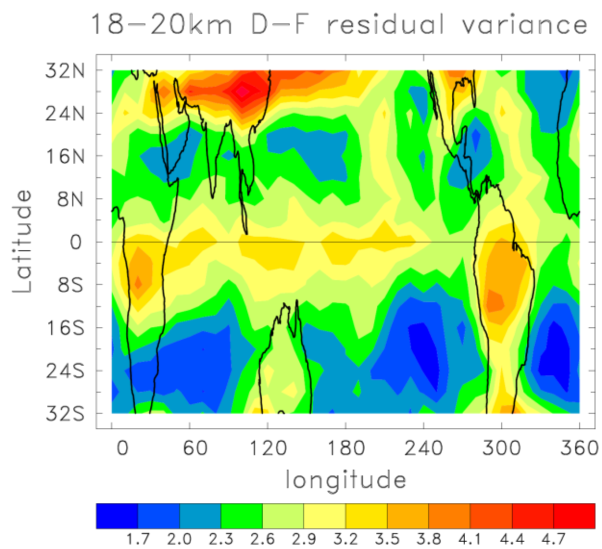

Figure 8. Time average (December-February) residual temperature variance (K^2) for the 18-20 km layer.

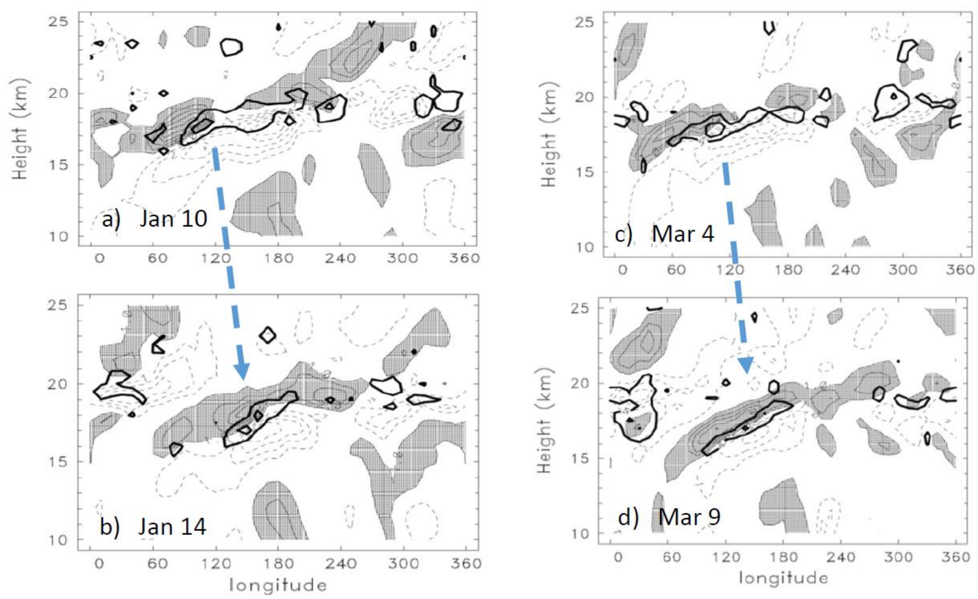

Figure 9. Cross sections showing the relationship of small-scale residual temperature variance near the equator (dark lines with contour interval of 4 K^2) with large-scale 'background' gridded temperature anomalies (light lines, contours of +/- 1,2,3,…K). Two snapshots are shown for events in January (left) and March (right). The large-scale anomalies are primary associated with eastward propagating Kelvin waves. Residual variance maxima are sandwiched between strong gradients in the background field, and follow the eastward phase progression (blue arrows) for both events.